Intramolecular dynamics. III. Theoretical studies of the CH overtone spectra for benzene

Yongfeng Zhang and R. A. Marcus
Arthur Amos Noyes Laboratory of Chemical Physics, California Institute of Technology, Pasadena, California 91125[a)]

(Received 18 January 1991; accepted 6 July 1992)

The CH overtone spectra for $v_{CH}=1$, 2, and 3 for an intermediate sized molecule, benzene, and the related intramolecular vibrational dynamics are treated theoretically. For this purpose, an artificial intelligence (AI) search technique is employed, using the evaluation function developed in Part II. The curvilinear local-normal mode coordinate system discussed in Part I is also used. The main features of the theoretical spectra are in reasonable accord with those of the experimental ones. Results reflecting the important role of the symmetry of molecules even in their high energy states are described.

I. INTRODUCTION

In studies of intramolecular dynamics, benzene occupies an interesting position as a textbook example[1-3] of a molecule of intermediate size. It displays many of the phenomena exhibited in other intermediate size molecules, such as Fermi resonance, vibration–rotation coupling, and radiationless transitions.[1-7] The simulation of the CH overtone spectra for benzene has received considerable attention in recent years. Initial experimental studies at room temperature by Reddy *et al.*[5] indicated that these high overtone vibrational spectra ($v_{CH}=4$ and higher) have a very broad width (60–110 cm^{-1}) and that they have more or less structureless spectral profiles. At $v_{CH}=1$ to 3, the spectra have some structure. The width for $v_{CH}=3$ is 43 cm^{-1}. Using supersonic cooling of molecules and a nonlinear labeling spectroscopic technique, recent experimental studies of Page *et al.*[3] on fundamental and overtone spectra of benzene provided high-resolution spectra for the C–H stretches from $v_{CH}=1$ to $v_{CH}=3$. Fine structure with a resolution of ~ 1 cm^{-1} was observed in the spectra.[3] The widths of these spectral peaks at 5 K were very narrow, only several cm^{-1} (4 to 10 cm^{-1}). The room temperature widths were substantially larger (tens of cm^{-1}). Scotoni *et al.* [7] studied the overtone $v_{CH}=3$ for benzene at 20 K. Seven vibrational bands have been resolved. A significant part of the CH oscillator strength is borrowed by lines located on "red" side of the main peak.

Several theoretical investigations on the intramolecular dynamics in benzene have been performed using classical trajectories or diagonalization of a model quantum-mechanical Hamiltonian.[8-15] The results obtained did not match well the subsequently obtained data on the fine structure behavior. A direct quantum-mechanical calculation for C–H overtones, involving a more detailed Hamiltonian and a wider selection of quantum-mechanical zeroth-order states, may therefore provide some insight into this discrepancy. The availability of both quadratic force constants and cubic anharmonic force constants for benzene[16-19] provides one base for the present study. The use of an artificial intelligence (AI) search method[20-22] offers a possible route of selecting an important subset from the potentially millions of relevant states for use as a basis set in a quantum-mechanical study of vibrational spectra and intramolecular dynamics of benzene as well as in other many-atom molecules.

Results are obtained for the fundamental transition, $v_{CH}=0$ to $v_{CH}=1$, and for the $v_{CH}=2$ and $v_{CH}=3$ overtones of the C–H stretch in benzene. The theoretical treatment is outlined in Sec. II. The results are given and compared with experimental data in Secs. III and IV, respectively. Curvilinear normal modes (CNM) are used for $v_{CH}=1$ and curvilinear local-normal modes (CLNM) are used for $v_{CH}=2$ and $v_{CH}=3$. The results are discussed further in Sec. V.

II. THEORETICAL TREATMENT

A. Coordinates and Hamiltonian

The curvilinear local-normal modes of molecules, and a corresponding anharmonic Hamiltonian based on Wilson's theory,[2] have been discussed in Part I of the present series.[23] A Hamiltonian for benzene in the curvilinear local-normal mode coordinates, treating, the six CH stretches as local modes, is given in Part I. Evaluation functions for an AI search have been suggested in Part II[22] to explore, in part, the role of internal resonances in selecting the important subset of states, for these systems where the density of states is so large that resonances become widespread. In the present work these results are used in a quantum-mechanical calculation of vibrational spectrum of the C–H overtones of benzene for $v_{CH}=1$, 2, and 3 and of the associated intramolecular dynamics, for the 21 in-plane modes, by diagonalizing the Hamiltonian, using the subset of zeroth-order states obtained in the AI search.

With CLNM only a part, the normal block, of the **GF** matrix is initially in a diagonal form, **G** and **F** being the mass and quadratic force constant matrices. The anharmonic Hamiltonian in CLNM for a general molecule (benzene being a special case) is written as[22]

[a)]Contribution No. 8381.

 0021-9606/92/205283-13$006.00

$$H=\sum_{i=1}^{M} h_i+H', \tag{1}$$

where M is the number of modes considered, h_i is the zeroth-order Hamiltonian term

$$h_i=\begin{cases} -\frac{\hbar^2}{2}\frac{\partial^2}{\partial Q_i^2}+D_i[e^{-2\alpha_i Q_i}-2e^{-\alpha_i Q_i}] \\ \quad \text{for local modes;} \\ -\frac{\hbar^2}{2}\frac{\partial^2}{\partial Q_i^2}+\frac{1}{2}K_{ii}^{(2)}Q_i^2 \\ \quad \text{for normal modes,} \end{cases} \tag{2}$$

namely, Morse and harmonic oscillators are used for local and normal modes, respectively, and H' is the perturbation,

$$H'=H_{\text{quadratic}}+H_{\text{cubic}}+H_{\text{quartic}}+\cdots, \tag{3}$$

where

$$H_{\text{quadratic}}=H_k^{(2)}+H_v^{(2)}, \quad H_{\text{cubic}}=H_k^{(3)}+H_v^{(3)}, \quad H_{\text{quartic}}=H_k^{(3)}+H_v^{(4)}. \tag{4}$$

$H_{\text{quadratic}}$ arises from the off-diagonal elements of the matrix **G** (at the equilibrium configuraton) and of the quadratic force constant matrix **F**, since both matrices are no longer diagonal in CLNM, although the local blocks of these two matrices are diagonal. The off-diagonal parts of the two matrices, $H_k^{(2)}$ and $H_v^{(2)}$, may be termed the stationary kinetic coupling and the harmonic potential coupling, respectively. The H_{cubic} involves both a kinetic coupling $H_k^{(3)}$, which contains the first derivative of the **G** matrix, and the cubic anharmonic potential coupling, $H_v^{(3)}$, but not the diagonal contribution to the h_i for local modes. Similarly, H_{quartic} involves both a kinetic coupling $H_k^{(4)}$, which contains the second derivative of **G**, and the quartic anharmonic coupling, $H_v^{(4)}$. Detailed expressions for these perturbations are given in Part I.[23] For benzene, all α_i's and all D_i's in Eq. (2) are, of course, equal.

The quadratic force constants for benzene obtained by Ozkabak and Goodman,[19] and the cubic force constants calculated by Pulay, Fogarasi, and Boggs[16] were used in the present work. The diagonal and semidiagonal quartic force constant of C–H and C–C stretch modes for benzene were estimated following the procedure given in Part I.

To avoid problems with redundancy a set of nonredundant coordinates is used, the same as these employed by Pulay[16,17] and rather similar to those employed by Wilson.[2]

B. AI search

The AI search procedure discussed in Part II of the present series is used.[22] In this search the accepted zeroth-order states are classified by tiers. A tier-i state is accepted in the ith search level of the search procedure when it directly couples with the tier-$(i-1)$ state but either does not couple with lower tier states or the direct couplings to them are so weak (evaluation function below a certain minimum) that they can be ignored. An evaluation function is defined to make this statement a quantitative one. Starting from the given initial state, these tier states form the paths. In the AI search method, the qualified zeroth-order states are accepted based on paths. For the search of tier-2 states the beam search method[20–22] is used and for higher tier states the best-first search method[20–22] is employed. In defining the evaluation function for large systems, a resonance effect on the propagation of the influence of an tier-$(n-1)$ state on a tier-n one, noted in Part II, may occur. It is incorporated into the present expression for the evaluation function, treating it for simplicity, however, as an "isolated resonance."

The evaluation function for a tier-n state in a path is defined in Part II as C_n

$$C_n=W_2\left[\prod_{i=2}^{n}|a_{i-1,i}|f\xi(a_{i-1,i-1},a_{ii})\right]\eta(a_{33}), \tag{5}$$

where W_2 is the weight factor of the tier-2 state in the path; W_2 is evaluated by a population analysis of a prediagonalization procedure; $a_{i-1,i}$ is the coupling element between the state i and its parent state, the tier-$(i-1)$ state; f is the *tier factor*, which is introduced to discourage, for a given total number of selected states, long paths in favor of shorter ones, f is chosen in the present study to be 0.5; one choice for ξ is a form similar to that for series circuits

$$\xi_i=\frac{1}{2}\left[\frac{1}{|a_{ii}-a_{11}|+|a_{ii}-a_{i-1,i-1}|}\right], \tag{6a}$$

which could be contrasted with another form,

$$\xi_i=\frac{1}{2}\left[\frac{1}{|a_{ii}-a_{11}|}+\frac{1}{|a_{ii}-a_{i-1,i-1}|}\right]. \tag{6b}$$

η is a parameter, and, as given in one form in Part II, is dependent upon the difference between the energy of the tier-3 state to the nearest tier-3 resonance center (R_3), the resonance center width (τ), and parameters A and B,

$$\eta(a_{33})=1+A\exp[-B|a_{33}-R_3|/\tau]. \tag{6c}$$

The AI search was initiated using a particular wave function, which is given later for each of the excitations investigated, $v_{CH}=1,2$, or 3.

C. Spectra

In the calculation of the spectrum, the wave function for the ground state Ψ_0 and the dipole moment function were also needed. An AI search was performed using 100 states selected from 3000 states searched in an energy range of ± 800 cm^{-1} centered about 18 255 cm^{-1}. In this search process Φ_0, the zeroth-order vibrational state of benzene with no vibrational quanta, was taken as the initial state. This search and diagonalization led to the eigenfunction of the ground state as being Ψ_0,

$$\Psi_0=0.9344\Phi_0-0.2713\phi_1+0.2171\phi_2+0.0658\phi_1^2-0.0179\phi_1^3, \tag{7}$$

where ϕ_1^i denotes a state with i quanta in model 1, for $i>1$. A relative transition intensity from the ground state to the

eigenstates Ψ_i around the 3000 cm^{-1} region can be calculated using the matrix element

$$I_i = |\langle \Psi_i | \mu | \Psi_0 \rangle|^2. \tag{8}$$

In general, the dipole moment operator μ can be expanded in normal modes,

$$\mu = \mu_0 + \sum_k \left(\frac{\partial \mu}{\partial Q_k}\right) Q_k + \sum_{k,k'} \left(\frac{\partial^2 \mu}{\partial Q_k \partial Q_{k'}}\right) Q_k Q_{k'} + \cdots. \tag{9}$$

Since the irreducible representations for the components of the dipole moment of benzene are A_{2u} and E_{1u}, a number of terms in the above summation vanish. When Eq. (9) is truncated to the linear term, the simplification provided by the symmetry then yields (in Wilson's numbering),

$$\mu \approx \mu_0 + \mu_{11}^{(1)} Q_{11}\mathbf{k} + \sum_{m=18}^{20} [\mu_{ma}^{(1)} Q_{ma}\mathbf{i} + \mu_{mb}^{(1)} Q_{mb}\mathbf{j}], \tag{10}$$

where **i**, **j**, **k** are the unit vectors along the x, y, and z directions, and Q_{11}, Q_{ma}, Q_{mb} refer to the modes Q_{11}, Q_{ma}, Q_{mb}. Q_{11} describes the z component of the dipole moment vector, since Q_{11} has the same transformation character as a unit vector along the z direction, **k**. Both Q_{11} and **k** belong to A_{2u} irreducible representation of D_{6h} group. Similarly, Q_{ma} and Q_{mb} ($m=18$, 19, and 20) have the same transformation character as the unit vectors of x and y direction, **i** and **j**. Therefore, the summation term in Eq. (10) is composed of the x and y contributions to the vector μ.

These values $\mu_{11}^{(1)}$, $\mu_{ma}^{(1)}$, and $\mu_{mb}^{(1)}$ of the nonzero derivatives of the dipole moment with respect to Q_1, Q_{ma}, and Q_{mb} for benzene have been calculated by Pulay *et al.*[16] Our resulting numerical calculations showed that the transition moment in the (x,y) plane arose almost entirely from the contribution of the E_{1u} C–H stretching mode, namely, $Q_{20a,b}$. In that case, only the $\mu_{20a}^{(1)} Q_{20a} + \mu_{20b}^{(1)} Q_{20b}$ term in Eq. (10) makes a significant contribution and so the absolute values of this term, which appears in Eq. (8), would not substantially affect the relative intensities in the infrared spectrum. Sibert *et al.*[9] also used such an approximation in their study of CH overtone spectrum of benzene. In our calculation, only in-plane modes were considered and so the $\mu_{11}^{(1)}$ term in Eq. (10) makes no contribution.

D. Energy flow

The eigenstates of the system are calculated here as linear combinations of zeroth-order states,

$$\Psi_k = \sum_i a_{ki} \Phi_i, \tag{11}$$

where Φ_i denotes the ith zeroth-order wave function of all the coordinates. A time-dependent wave function $\chi(t)$ of the systems is determined by a prepared state χ_0 at $t=0$

$$\chi_0 = \sum_j b_j \Phi_j, \tag{12}$$

and the time evolution is given by

$$\chi(t) = e^{-iHt/\hbar} \chi_0. \tag{13}$$

In treating an energy flow of a system to or from a zeroth-order mode, an "energy" for the kth mode can be defined as

$$\epsilon_k(t) = \langle \chi(t) | h_k | \chi(t) \rangle, \tag{14}$$

where $\chi(t)$ is the time-dependent wave function of the system, given in Eq. (13) and h_k is defined in Eqs. (1) and (2). From Eqs. (11)–(14) we have

$$\epsilon_k(t) = \sum_i \epsilon_i^k \rho_i(t), \tag{15}$$

where the sum is over contributions from the zeroth-order wave functions Φ_i considered and where

$$\epsilon_i^k = \langle \Phi_i | h_k(Q_k) | \Phi_i \rangle, \tag{16}$$

and

$$\rho_i(t) = \left| \sum_{j,m} a_{mi} a_{mj}^* b_j e^{-iE_m t/\hbar} \right|^2. \tag{17}$$

Equation (15) is the equation used to calculate the energy flow in this study.

A Fourier transformation of these energy flows,

$$\tilde{\epsilon}_k(\nu) = \int_0^\infty \epsilon_k(t) e^{2\pi i \nu t}\, dt, \tag{18}$$

can show the periodic structure of energy flows explicitly. Another quantity for examining the intramolecular dynamics used here is the initial state projection $P(t)$, defined as

$$P(t) = \langle \chi_0 | \chi(t) \rangle. \tag{19}$$

$P(t)$ describes the projection of the wave function at time t on an initially prepared wave function χ_0.

III. RESULTS FOR FUNDAMENTAL TRANSITION OF C–H MODES

Using the potential energy and kinetic coupling picture for benzene given in Part I,[23] the AI search method,[20,21] and the evaluation function given in Part II,[22] the fundamental transition for benzene, from $v_{CH}=0$ to $v_{CH}=1$ was calculated. Since this transition involves only lower vibrational quanta, normal mode coordinates rather than the CLNM provided a good scheme. In this case there is no local mode block.[23] For this calculation, the cubic force constants, and the first derivatives of the **G** matrix were included. The harmonic force field, obtained by Ozkabak and Goodman[19] from experimental frequencies for D_{6h}, D_{3h}, and D_{2h} isotopically labeled benzenes and degenerate mode Coriolis constants, was used, together with the cubic potential parameters for the ground state of benzene calculated by Pulay *et al.*[16] The Hamiltonian used is discussed in detail in Part I.[23] The numbers of terms in each type of perturbation term in the Hamiltonian are given in Table I. In total, 4310 such perturbation terms are considered here. In the AI search procedure, cognizance is taken of the resonance centers (RC) in tier-2 by a prediagonalization procedure and of an RC shift effect[22] in tier-3.

TABLE I. Numbers of perturbation terms for AI search calculation of benzene.[a,b]

Perturbation[a]	Threshold[c]	Normal modes ($l=0$)	Local-normal modes ($l=6$)
$H_k^{(2)}$		0	52
$H_v^{(2)}$		0	67
$H_k^{(3)}$	0.01 cm^{-1} Å	948	1678
$H_v^{(3)}$	0.01 cm^{-1} $Å^{-3}$	585	983
$H_k^{(4)}$	0.05 cm^{-1}	2336	1931
$H_v^{(4)}$	0.12 cm^{-1} $Å^{-4}$	441	534
Total		4310	5245

[a]For notation see Eq. (3) in Sec. I. Details are given in Part I.
[b]l is the size of local block, as is defined in Part I.
[c]Terms smaller than this threshold are omitted.

A. Eigenvectors and spectrum

For benzene there is a well-known Fermi resonance[1-7] in the region of 3000 cm^{-1}. It has been observed that there are three strong absorption peaks in this spectral region,[3,7] as shown in Fig. 1(b). These peaks are usually assigned as the result of interaction of the fundamental ϕ_{20} with two combination modes,[1-7] $\phi_{1\ 6\ 19}$ and $\phi_{8\ 19}$, where $\phi_{i\ j\ k}$ denotes the zeroth-order wave function of all the coordinates in which i, j, and kth zeroth-order single mode wave functions are singly excited and others are unexcited. Wilson's numbering scheme,[2,3,7] given in Table III of Ref. 23, is used for vibrational modes. All of these modes are in-plane modes.

In the AI search procedure used for the fundamental transition of benzene, some 382 important zeroth-order states were selected from 113 364 states in an energy range of ± 800 cm^{-1}, centered about ϕ_{20a} and ϕ_{20b}. The sum $\phi_{20a}+\phi_{20b}$ was used as the initial state. (ϕ_{20a} and ϕ_{20b} were considered individually, the results for the sum obtained, and redundancies in states removed.) The quantum mechanical Hamiltonian was then diagonalized using this subset of states, yielding a 382×382 matrix for the eigenvalues and eigenstates, the latter denoted by Ψ_i.

By using the eigenfunctions obtained for the region of 3000 cm^{-1} Eq. (7) for the ground state eigenfunction Ψ_0, Eqs. (8) and (10) the corresponding spectrum in the 3000 cm^{-1} region was calculated and is given in Fig. 1(a).

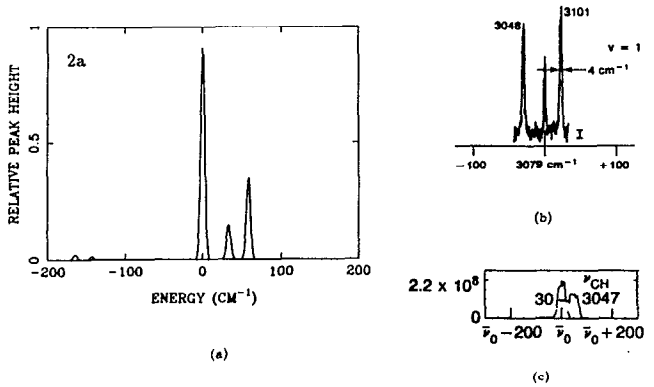

FIG. 1. The vibrational spectrum of $v=1$ for benzene: (a) Theoretical result by using AI search procedure, (b) experimental, Ref. 7, (c) experimental, Ref. 5.

The six principal eigenstates, or three pairs of nearly degenerate eigenstates, which correspond to the three strong infrared spectrum peaks in 3000 cm^{-1} region are obtained in the present calculation as the following. Only the ϕ's with coefficients greater than 0.05 are given below, but the complete Ψ's are used in the actual calculations. The same remark applies to all other Ψ's in this article.

$$\Psi_{1a}=0.786\phi_{20a}+0.400[-\phi_{8a\ 19a}+\phi_{8b\ 19b}]+0.147\phi_{8b\ 14}$$
$$+0.116[-\phi_{1\ 6a\ 19a}+\phi_{1\ 6b\ 19b}]-0.058\phi_{3\ 19b},$$
$$\Psi_{1b}=0.787\phi_{20b}+0.400[\phi_{8a\ 19a}+\phi_{8b\ 19b}]-0.147\phi_{8a\ 14}$$
$$+0.117[\phi_{1\ 6a\ 19a}+\phi_{1\ 6b\ 19b}]+0.058\phi_{3\ 19a},$$
$$\Psi_{2a}=0.645[-\phi_{1\ 6a\ 19a}+\phi_{1\ 6b\ 19b}]-0.321\phi_{20a}+0.133$$
$$\times[-\phi_{8a\ 19a}+\phi_{8b\ 19b}]-0.075[\phi_{1\ 6a\ 18a}^{1\ 2\ 1}+\phi_{1\ 6b\ 18a}^{1\ 2\ 1}], \quad (20)$$
$$\Psi_{2b}=0.645[\phi_{1\ 6a\ 19a}+\phi_{1\ 6b\ 19b}]-0.321\phi_{20b}$$
$$+0.133[\phi_{8a\ 19a}+\phi_{8b\ 19b}]$$
$$-0.075[\phi_{1\ 6a\ 18b}^{1\ 2\ 1}+\phi_{1\ 6b\ 18b}^{1\ 2\ 1}],$$
$$\Psi_{3a}=0.555[-\phi_{8a\ 19a}+\phi_{8b\ 19b}]-0.490\phi_{20a}$$
$$-0.235[-\phi_{1\ 6a\ 19a}+\phi_{1\ 6b\ 19b}],$$
$$\Psi_{3b}=0.555[\phi_{8a\ 19a}+\phi_{8b\ 19b}]-0.490\phi_{20b}$$
$$-0.235[\phi_{1\ 6a\ 19a}+\phi_{1\ 6b\ 19b}],$$

where the superscripts 1, 2, 1 appearing in terms in the Ψ_{2a} and Ψ_{2b} indicate that modes 1 and 18a or 18b are singly excited and mode 6a or 6b is doubly excited. Using group theory for power spaces, we have shown that these three pairs of states are exactly doubly degenerate.[24] They form an E_{1u} irreducible representation of the D_{6h} group, and will be discussed in detail in a later paper.[24] Numerical results obtained here also show their degeneracy. This point also indicates that the numerical results are reliable. (The numerical errors are reflected in minor differences of the coefficients in Ψ_{1a} and Ψ_{1b}.) The present results lend added support to the previous assignment,[1-7] now using an *ab initio* anharmonic coupling calculation, that the Fermi resonance is due mainly to interaction among the zeroth-order states ϕ_{20}, $\phi_{1\ 6\ 19}$, and $\phi_{8\ 19}$.

Comparing with experimental results shown in Figs. 1(b) and 1(c), the theoretical spectrum is seen to be in reasonable agreement with them. The results in Fig. 1(b) are the recent precise experimental ones of Page *et al.*,[3,7] which were obtained at about 5 K.

Two very weak peaks, near 150 and 170 cm^{-1} to the red of the strongest peak of the spectrum, appear in the present calculation, as seen in Fig. 1(a). The corresponding eigenfunctions form two pairs of degenerate states, whose degeneracy will be shown exactly in the later work.[24] They are

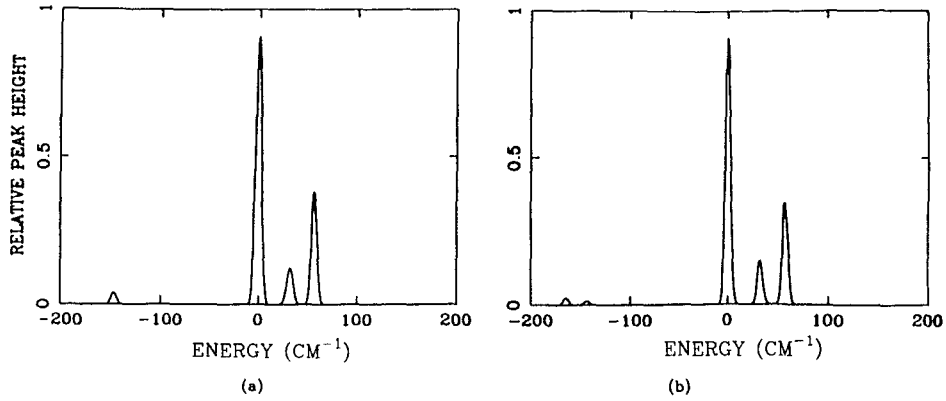

FIG. 2. Convergency of the AI search method for $v=1$: (a) 100 states chosen from 30 162 states, (b) 382 states chosen from 113 364 states.

$$\begin{aligned}
\Psi_{4a}&=0.805\phi_{8b\ 14}+0.550\phi_{1\ 6b\ 14}+0.122\phi_{20a}\,,\\
\Psi_{4b}&=0.805\phi_{8a\ 14}+0.550\phi_{1\ 6a\ 14}+0.122\phi_{20b}\,,\\
\Psi_{5a}&=0.814\phi_{1\ 6b\ 14}-0.540\phi_{8b\ 14}+0.094\phi_{20a}\,,\\
\Psi_{5b}&=0.814\phi_{1\ 6a\ 14}-0.540\phi_{8a\ 14}-0.094\phi_{20b}\,.
\end{aligned} \tag{21}$$

These two weak peaks were observed experimentally by Brodersen and Langseth,[4] who assigned them as a double Fermi resonance between $\phi_{(8a,b)\ 14}$ and $\phi_{1\ (6a,b)\ 14}$. This assignment is also supported, as seen in Eq. (21), by the present calculation. However, it is also seen that for the potential energy function used these states are also weakly mixed with $\phi_{(20a,b)}$. Actually, it is these small components of $\phi_{(20a,b)}$ which are the source of the transition intensities for these states in the present calculation.

When fewer states were collected in the AI search, the broad picture for the spectrum did not change. A comparison, for example, is given in Fig. 2, between the cases where 100 states were collected from 30 162 states and where 382 states were selected from 113 364 states. The three main peaks in this region are the same. This result indicates that the AI search procedure is, in effect, "converged" for the three principal peaks. However, one of the two weak peaks in the 382-states case does not appear in the 100-state one. This indicates that the more thorough AI search provides, as expected, a more complete description. The results were almost the same, regardless of whether Eq. (6a) or (6b) was used.

B. Coupling manifold

We examine next the coupling manifold of the triple Fermi resonance among the ϕ_{20}, $\phi_{8\ 19}$, and $\phi_{1\ 6\ 19}$ states. The three zeroth-order energy levels and those obtained in the calculation, after applying a zero-point energy correction,[25] are given in Figs. 3(a) and 3(b), respectively. They are compared with the experimental values in Fig. 3(c).

In Fig. 4 the coupling chain is shown for the main path of this calculation. In the AI search tree for the excited states, $\phi_{20}^{a,b}$ is the initial state, a CH stretching excitation, $\phi_{8\ 19}$ is a tier-2 state of the main path, and $\phi_{1\ 6\ 19}$ is a tier-3 state. The calculated coupling matrix elements between the states are

$$\begin{aligned}
&\langle\phi_{20}|H'|\phi_{8\ 19}\rangle=18\ \text{cm}^{-1}\\
&\langle\phi_{8\ 19}|H'|\phi_{1\ 6\ 19}\rangle=10\ \text{cm}^{-1}.
\end{aligned} \tag{22}$$

The calculated matrix elements are in agreement with those fitted to the experimental data by Pliva and Pine, 23 and 9 cm^{-1}, respectively.[11,26] Those authors attributed the observed couplings between these states as due to the cubic anharmonic force constants, $K^{(3)}_{8,19,20}$ for $\langle\phi_{20}|H'|\phi_{8\ 19}\rangle$ and $K^{(3)}_{1,6,8}$ for $\langle\phi_{8\ 19}|H'|\phi_{1\ 6\ 19}\rangle$. In the present *ab initio* calculation, it was indeed observed that the source for the coupling element $\langle\phi_{8\ 19}|H'|\phi_{1\ 6\ 19}\rangle$ is due to the cubic anharmonic coupling,

$$H^{(3)}_{v;1,6,8}=K^{(3)}_{1,6,8}Q_1Q_6Q_8\,, \tag{23}$$

a *tαt* type cubic anharmonic coupling, where the cubic terms are characterized by types of principal internal coordinate components of the modes *s*, *t*, α, β, etc., as defined in Part I:[23] *s* denotes CH stretch, *t* CC stretch, α is CCC valence bend and β is CCH in-plane wag. However, in the present curvilinear coordinate treatment the coupling ele-

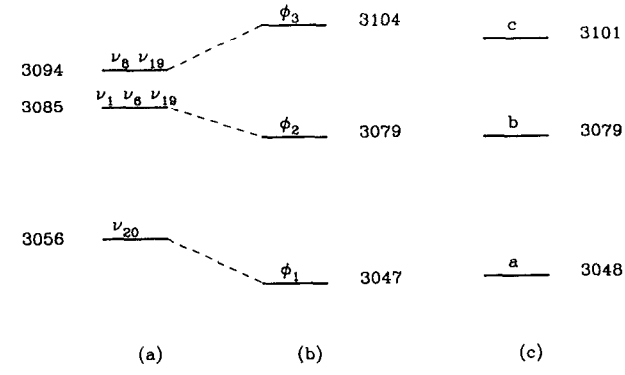

FIG. 3. Triple Fermi resonance near 3000 cm^{-1} for benzene: (a) Zeroth-order energy levels, (b) theoretical energy levels, (c) experimental data.

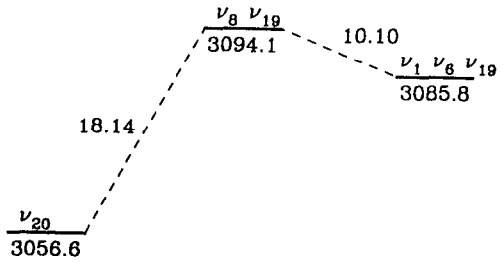

FIG. 4. Main path of AI search for $v_{CH}=1$ of benzene.

ment $\langle\phi_{20}|H'|\phi_{8\ 19}\rangle$ is, due instead to first-order kinetic couplings, rather than to the cubic anharmonic coupling $K^{(3)}_{8,19,20}$,

$$H^{(3)}_{k;8,19,20}=W^{(1)}_{8,19,20}P_8Q_{19}P_{20}+W^{(1)}_{19,8,20}P_{19}Q_8P_{20}+W^{(1)}_{8,20,19}P_8Q_{20}P_{19}\,, \tag{24}$$

which has *tst* and *stt*-type kinetic couplings. Had we employed Cartesian normal modes instead of curvilinear ones, the only cubic coupling involving these modes would have been $K^{(3)}_{8,19,20}$ (cf. Ref. 27 for a comparison of curvilinear and Cartesian formulations).

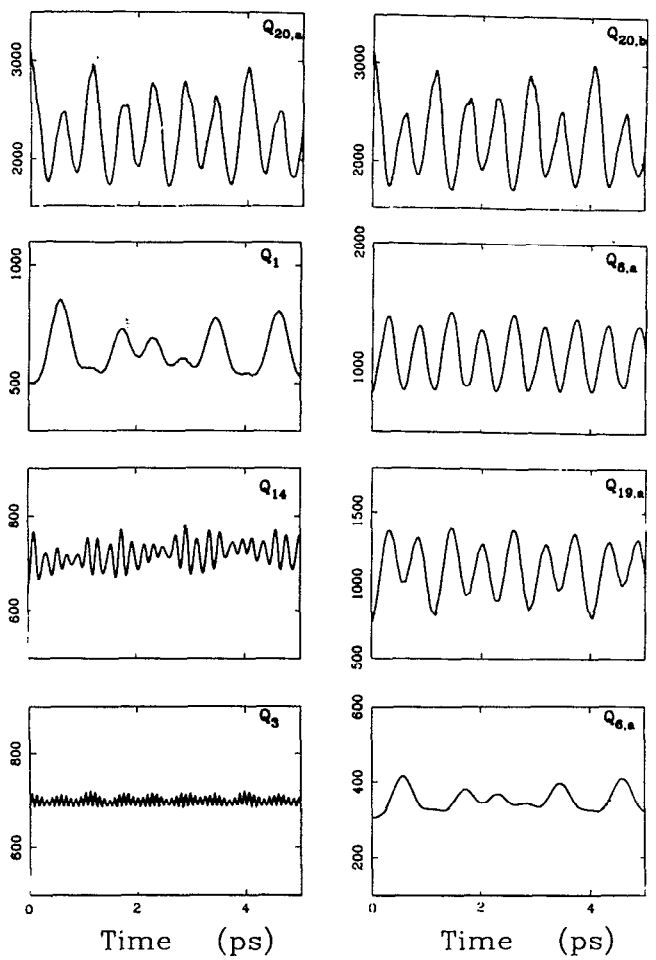

FIG. 5. Energy flows $\epsilon_k(t)$ for some modes of benzene near 3000 cm^{-1}, small time scale, 5 ps, in Wilson's numbering.

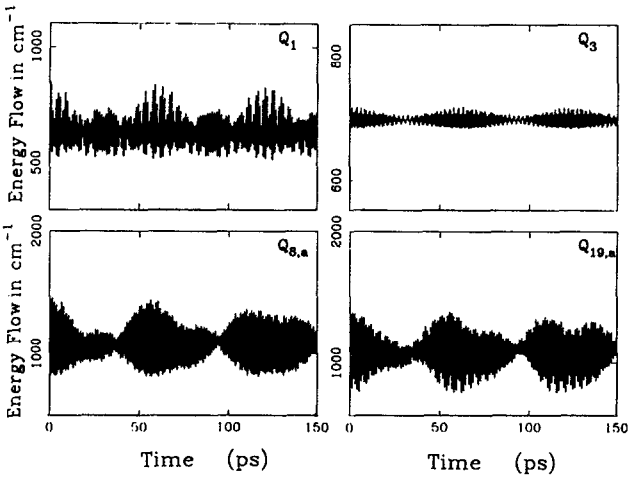

FIG. 6. Energy flows $\epsilon_k(t)$ for some modes of benzene near 3000 cm^{-1}, large time scale, 150 ps, in Wilson's numbering.

In summary, the main anharmonic coupling feature is *tst, stt,* and *tαt*, i.e. C–H stretching (s) is coupled to C–C stretching (t) and to CCC angle bending (α), and is, in part, potential $H^{(3)}_{v;1,6,8}$ and, in part, in the present formalism, kinetic coupling $W^{(1)}_{8,19,20}$, $W^{(1)}_{19,8,20}$, and $W^{(1)}_{8,20,19}$.

C. Energy flow and initial state projection

For the fundamental transition around 3000 cm^{-1} for benzene we consider an initially prepared state χ_0 localized in $\phi_{(20a,b)}$,

$$\chi_0=\frac{1}{\sqrt{2}}\left[\phi_{20a}+\phi_{20b}\right] \tag{25}$$

and obtain the energy flow for each in-plane mode of benzene using Eq. (15). Upon examining the results, it is found that only seven modes have nontrivial energy flows in the present calculation. These seven modes are (in Wilson's numbering) Q_1, Q_3, Q_6, Q_8, Q_{14}, Q_{19}, and Q_{20} as seen from Eq. (20). Indeed, these modes are ones principally involved in the triple Fermi resonance.

The time behavior of these energy flows for these modes is depicted in Fig. 5 for short times and in Fig. 6 for longer times. Some periodicity is evident, as expected from the few number of modes involved. The main peaks of the Fourier transforms $\tilde{\epsilon}_k(\nu)$ of these energy flows, calculated using Eq. (18), are shown in Table II. The Fourier transformation of the energy flows for Q_{20}, Q_{19}, Q_8, and Q_1 are shown in Fig. 7. From these calculations it can be seen that the most important contribution to the energy flow has a period of 0.58 ps. In this energy flow contribution, the vibrational energy oscillates back and forth largely between Q_{20}, Q_8, and Q_{19}, with some contribution from Q_1. Thereby, it oscillates between C–H stretching and C–C stretching, the latter mixed with the other (CC and CCH) motions. The period of 0.58 ps corresponds to 57 cm^{-1} and so to the theoretically calculated difference frequency

TABLE II. Important periods for Fourier energy flow $\tilde{\epsilon}_k(\nu)$ for $v_{CH}=1$ of benzene.[a]

Mode and its main displacement		Period (ps)	$\tilde{\epsilon}_k(\nu)$
ν_{30}	C–H stretching	1.3	36.1
		1.0	89.7
		0.58	231.9
		0.46	4.7
		0.23	8.7
		0.20	13.3
		0.15	9.8
ν_8	C–C stretching	1.3	14.2
		1.0	15.4
		0.58	70.1
		0.23	4.4
		0.20	7.6
		0.15	4.7
ν_{14}	C–C stretching	0.23	4.3
		0.20	6.3
		0.15	3.7
ν_{19}	C–C stretching	1.3	14.3
		1.0	22.7
		0.58	57.4
ν_1	C–C stretching	1.3	43.0
		1.0	17.8
		0.58	11.2

[a] $\tilde{\epsilon}_k(\nu)$ is calculated using Eq. (18).

(3104–3047) of the two main peaks in Fig. 1 (cf. Fig. 3). Experimentally, this difference frequency is equal to 53 cm^{-1}, i.e., (3101–3048).[7] There is also a longer time period, seen to be about 60 ps in Fig. 6. It corresponds to a side band splitting in the Fourier transform of about 0.05 cm^{-1}.

The results for the initial state projection $P(t)$ for the C–H mode at short and at long times, calculated using Eq. (19), are shown in Figs. 8 and 9, respectively. At short times (0 to 0.15 ps), shown in Fig. 8, the decay is sharp and approximately linear in t. However, on a long time scale ($\sim$5 ps), both the initial decay and a periodic structure are seen as in Fig. 9.

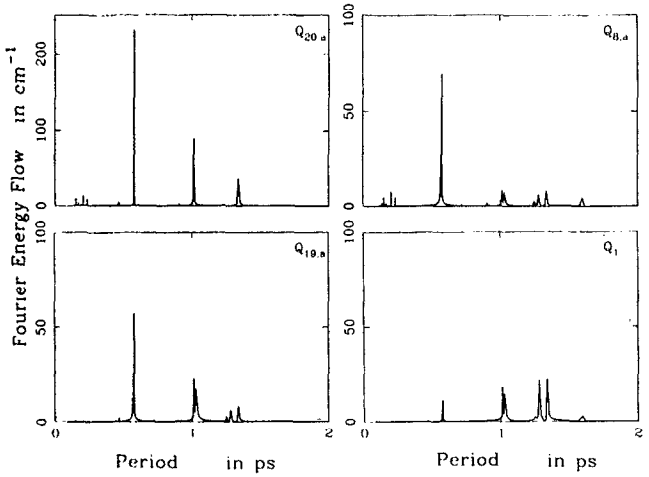

FIG. 7. Fourier energy flows $\tilde{\epsilon}_k(\nu)$ for some modes of benzene near 3000 cm^{-1}, in Wilson's numbering.

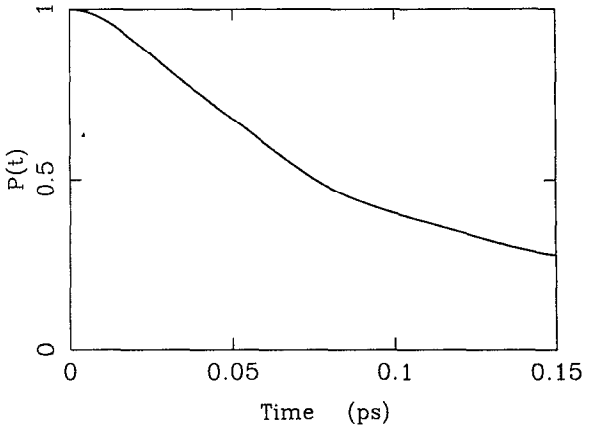

FIG. 8. Initial state projection $P(t)$ for benzene near 3000 cm^{-1}, smaller time scale, 0.15 ps.

IV. RESULTS FOR C–H OVERTONES FOR $v_{CH}=2$ AND $v_{CH}=3$

The C–H overtone transitions for benzene for $v_{CH}=0$ to 2 and 3, involve higher vibrational quanta, and the curvilinear normal-local modes provide a better starting description than a purely curvilinear normal mode description. In this case the six C–H stretching modes are treated here as local modes, and remaining other in-plane modes as CNM's. As a result, there is a 6×6 local mode block and a 15×15 normal mode block in the $\mathbf{G}^{(0)}\mathbf{F}^{(2)}$ matrix, as discussed in Ref. 23. For this case, the off-diagonal blocks of the transformed $\mathbf{G}^{(0)}\mathbf{F}^{(2)}$ matrix to CLNM contain, in addition to the cubic and quartic force constants, the first and second derivatives of the $\mathbf{G}$ matrix. The numbers of terms in each perturbation Hamiltonian are given in Table I. In total, 5245 perturbation terms are considered here.

Since the CLNM are used here, the expression of Hamiltonian differs from that for the CNM. In order to calculate the radiative transition rate from the ground state to these excited states, the wave function of the ground state is expressed in terms of the same scheme. Using an AI

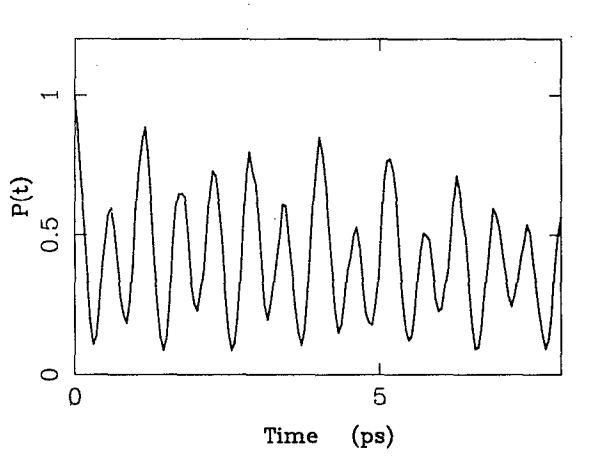

FIG. 9. Initial state projection $P(t)$ for benzene near 3000 cm^{-1}, larger time scale, 8 ps.

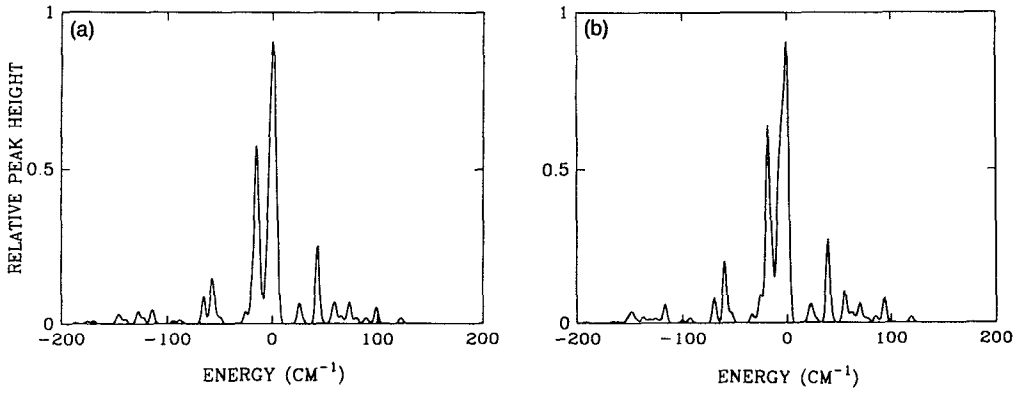

FIG. 10. Convergency of the AI search method for $v_{CH}=2$: Spectrum for $v_{CH}=0$ to $v_{CH}=2$ calculated from (a) 517 states chosen from 92 873 states, (b) 1000 states chosen from 166 694 states.

search, the wave function of the ground state was obtained in the CLNM (using the L numbering in Table III of Part I[23]) as

$$\Psi_0=0.9417\Phi_0+0.2773\phi_7+0.0327[\phi_{1\ 15}-\phi_{2\ 15}+\phi_{3\ 15}-\phi_{4\ 15}-\phi_{5\ 15}+\phi_{6\ 15}], \quad (26)$$

where Φ_0 is the zeroth-order state whose quanta all are zero. In comparing this expression with Eq. (7) for Ψ_0, it may be noted that because of the difference in coordinates [Eq. (7) uses only normal modes], the wave functions Φ_0, ϕ_7, and the others in Eq. (7) differ from those in Eq. (26).

A. AI search and its convergence

The AI search method for these C–H overtone transitions of benzene was again used. As in the previous section, the search was performed and a subset of important states was obtained. The Hamiltonian was then diagonalized using this subset, so yielding the eigenvalues and eigenstates. The vibrational spectrum of various spectral transitions may be calculated, based on either the dipole moment operator of Eq. (9) or using, because of the larger CH extensions now, the bond dipole model.[28,29] The details are given in the Appendix. For $v_{CH}=2$, the AI search was used to select 250 important zeroth-order states from 92 893 states. In this search, the doubly excited zeroth-order states of the six CH stretching local modes, ϕ_j^2 where $j=1,\cdots 6$ in L numbering, were used as the initial states. The sum $\Sigma\phi_j^2$, $j=1$ to 6, served as the initial state. (Each ϕ_j^2 was considered individually and the results for the sum obtained, and redundancies in states removed.) The eigenvectors were then obtained by diagonalization of the Hamiltonian matrix using these 250 states. In order to explore the "convergence" of the AI search, a calculation for $v_{CH}=2$ was also performed in which 1000 important states were selected from 447 094 states, in an energy range of ± 800 cm^{-1}, centered about 24 473 cm^{-1}. The two spectra are compared in Fig. 10, broadened slightly by using a rotational temperature of 5 K. These two theoretical spectra are seen to be fairly similar, but with the largest peak now showing a shoulder in the 1000-state case.

A comparison between the experimental and theoretical spectra for $v_{CH}=2$ is given in Fig. 11, where the experimental result of Page *et al.*[3,7] at low temperature (5 K) is also given: There is a main peak with width of 4 cm^{-1} and a second peak on the red side. The theoretical width is about 5 cm^{-1}. (The rotational broadening at 5 K contributes about 4 cm^{-1}.[7]) Some of the experimental weaker peaks on the red side of these peaks did not appear in the calculated spectrum. The results using Eq. (6a) were almost the same as those in Fig. 11, obtained using Eq. (6b).

For $v_{CH}=3$, the density of states of the 21 in-plane vibrations is high, about 420 states per cm^{-1}. In the AI search 1000 important zeroth-order states were selected from 1 329 044 states in an energy range of ± 800 cm^{-1}, centered about 27 277 cm^{-1}. In this search, the sum $\Sigma_j\phi_j^3$ of the triply excited zeroth-order states on the six CH stretching local modes, ϕ_j^3, where $j=1,\cdots 6$ in L numbering, served as the initial state. The eigenvectors were again obtained by diagonalization of the Hamiltonian matrix using these 1000 states. The resulting theoretical spectrum for a rotational temperature of 5 K is shown in Fig. 12(a). The width of the main peak is about 9 cm^{-1}, while the experimental result is 10 cm^{-1} at this low temperature[3,7] [Fig. 12(b)]. In Fig. 12(b), the experimentally obtained peaks other than the main peak (8827 cm^{-1}) are very weak. However, in Fig. 12(a), a few theoretical peaks appear somewhat stronger.

In the AI search, Eq. (6b) and the values of $A=1$ and $B=0.5$ in Eq. (6c) were used. Results obtained with other conditions [Eq. (6a) or other values of B] are given in a later section.

The approximations made in the theory involve the potential energy parameters, the truncation of the kinetic energy expansion, the restriction of the AI search, restriction to in-plane vibrations, and the treatment of the rotation. Further *ab initio* studies of the anharmonic constants of benzene[30] are in progress. When these constants become available, they can be used in the present calculation. In the present study the main peak of the low-temperature spectrum is seen to correspond to many eigenstates. With

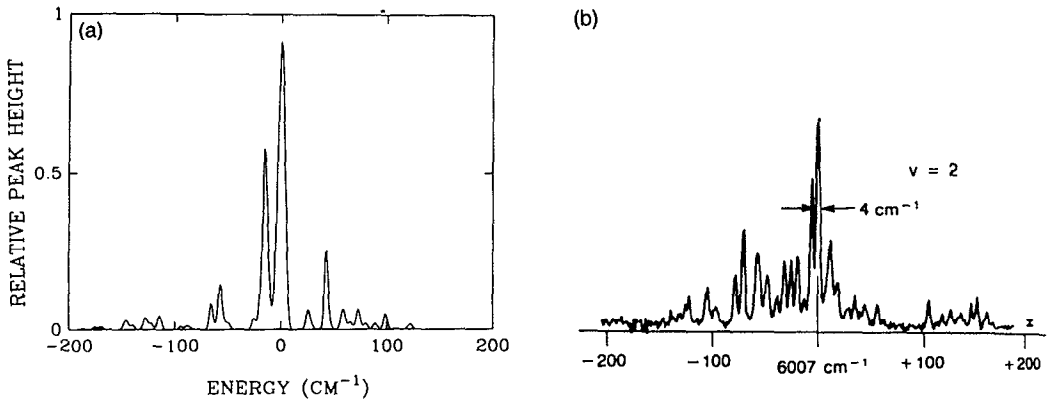

FIG. 11. The vibrational spectrum of $v_{CH}=0$ to $v_{CH}=2$ for benzene: (a) Theoretical result using AI search procedure, (b) experimental, Ref. 7.

higher resolution results on these states may be distinguished.

B. Energy flow $\epsilon_K(t)$ and $\tilde{\epsilon}_K(\nu)$ and initial state projection $P(t)$

The energy flow for the transition $v_{CH}=0$ to $v_{CH}=3$ has been calculated using the eigenfunctions obtained and Eqs. (15)–(17). A representative initial state for the energy flow for $v_{CH}=3$ is taken to be (in L numbering)

$$\chi_0=[\phi_1^3+\phi_2^3+\phi_3^3+\phi_4^3+\phi_5^3+\phi_6^3]/\sqrt{6}. \tag{27}$$

The principal feature of the energy flow for $v_{CH}=3$ differs from that for $v_{CH}=1$. For the latter, there are only seven modes which have nontrivial energy flows. However, for the former, almost all of the modes have nontrivial energy flows. These flows for some modes for the $v_{CH}=3$ system are shown in Fig. 13.

One important phenomenon is seen in Fig. 13: Degenerate modes have similar energy flows. The behavior of three pairs of degenerate modes, $\{Q_{11},Q_{12}\}$, $\{Q_{13},Q_{14}\}$, and $\{Q_{17},Q_{18}\}$ is shown in Fig. 13, and each member of a pair is seen to behave similarly within the numerical approximation. This result (and subsequent analytic work) imply that processes involving high overtones, or strongly anharmonic systems still retain the symmetry character in the ground state. Namely, no anharmonic coupling removes the molecular symmetry, as long as the vibrational energy is not so high that the nuclei actually exchange their positions in the time scale of interest.

This phenomenon of similar behavior of the degenerate pairs provides a motivation for combining the AI search with symmetry considerations to study these higher overtone processes. Specifically, it is not necessary to perform the search on the whole state space (within some given energy range) for intramolecular processes. Performing an AI search in the appropriate symmetrical subspace suffices. For example, to study the one-photon absorption or fluorescence spectra of benzene it suffices to consider the states in the E_{1u} irreducible representation subspace. Actually, only one of the two components of E_{1u} needs to be considered. For overtone excitation processes the construction of the symmetric combinations is nontrivial to treat all of the symmetry correctly. Mathematically, this problem is one involving group representation theory on power spaces.

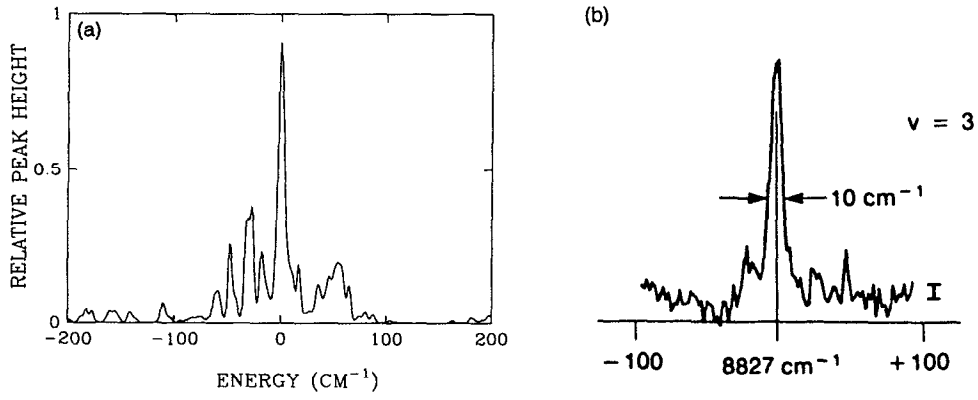

FIG. 12. The vibrational spectrum of $v_{CH}=0$ to $v_{CH}=3$ for benzene: (a) Theoretical result by using AI search procedure, (b) experimental, Ref. 7.

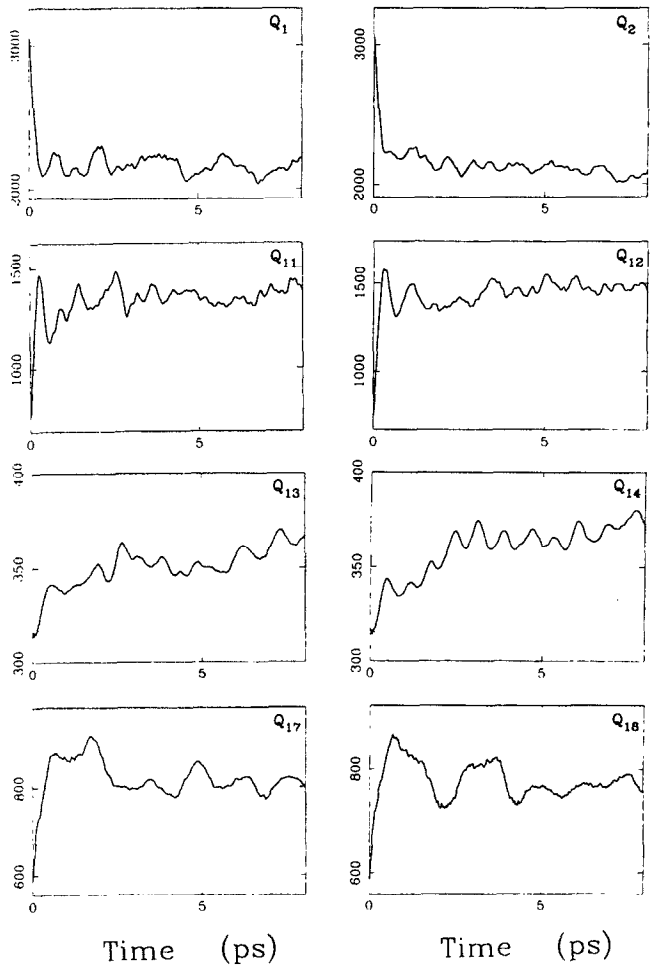

FIG. 13. Energy flows $\epsilon_k(t)$ for some modes of benzene near 9000 cm^{-1}, in local mode numbering.

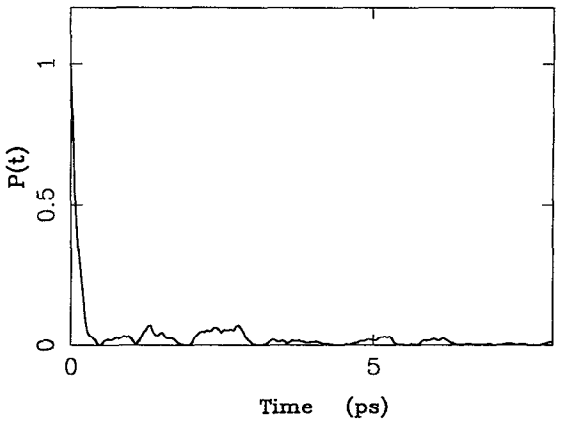

FIG. 14. Initial state projection $P(t)$ for benzene near 9000 cm^{-1}.

However, we have introduced in Part IV a concept of *true product coefficients* (TPC) for finite groups to obtain these combinations in power spaces. For example, it can be shown that the totally symmetric combination related to $Q_{7a}Q_{7b}^2$ is $Q_{7a}^3-3Q_{7a}Q_{7b}^2$. The details of definition, properties and applications of TPC will be given in Part IV of this series. This consideration of symmetry reduces the computational effort of the AI search-diagonalization procedure, and the new procedure will be discussed further there.

The initial state projection for $v_{CH}=3$ [initial state as Eq. (27)] is shown in Fig. 14, and a comparison of this dynamic quantity with that for $v_{CH}=1$ (Fig. 9) is of some interest: For $v_{CH}=1$, many oscillations follow the initial rapid decay. However, for $v_{CH}=3$ there are no strong oscillations after the initial decay. This difference reflects the more extensive "intramolecular vibrational relaxation" at the higher energy—many more states are significantly involved in the couplings to initially prepared state.

V. DISCUSSION

A. The importance of quartic couplings

Many calculations for the intramolecular dynamics of benzene have been described in the literature, either with classical trajectories or with a diagonalization of model quantum mechanical Hamiltonian.[8–15] For practical reasons, the quartic potential energy couplings were omitted. It seems appropriate to neglect quartic couplings for the $v_{CH}=1$ transition. The density of states at this energy range (3000 cm^{-1}) is very small, only 0.4 states per cm^{-1}. There is only one important Fermi resonance, a triple Fermi resonance, in the region involving the $v_{CH}=1$ excitation, and so the quartic coupling did not play any important role for $v_{CH}=1$. However, overtones involve higher energies and so the density of states is much higher. An increasing number of Fermi resonances, triple, quadruple even higher, may appear. As seen in the present work, the quartic couplings play a significant role, as illustrated in the spectra in Fig. 15 for $v_{CH}=3$ for calculations with and without quartic couplings (the quartic terms include the quartic kinetic energy couplings).

B. Kinetic couplings

In their treatment, Sibert *et al.* showed importance of the kinetic coupling,[9] and omitted in their study the contribution from cubic and other anharmonic force constants. Both cubic force constants and first-order kinetic couplings are needed, we have seen, for obtaining a correct description of the couplings, indeed even in the $v_{CH}=1$ transition. To emphasize this point of view, some comparison is given in Fig. 16, where the calculation for $v_{CH}=1$ with cubic force constants but without the first-order kinetic coupling is given in Fig. 16(a), while in Fig. 16(b) the first-order kinetic couplings but no cubic force constants are used, and in Fig. 16(c) both of them are used. It is evident that both of these couplings make significant contributions.

C. Other conditions for $v_{CH}=3$ search

We have explored the use of a different choice for the value of B in Eq. (6c), using Eq. (6b) as before. In Fig. 17 a comparison of calculated results for spectra of transition $v_{CH}=0$ to $v_{CH}=3$ with $B=0.1$ (solid line) and $B=0.5$ (dotted line), is given. The main peak of the experimental

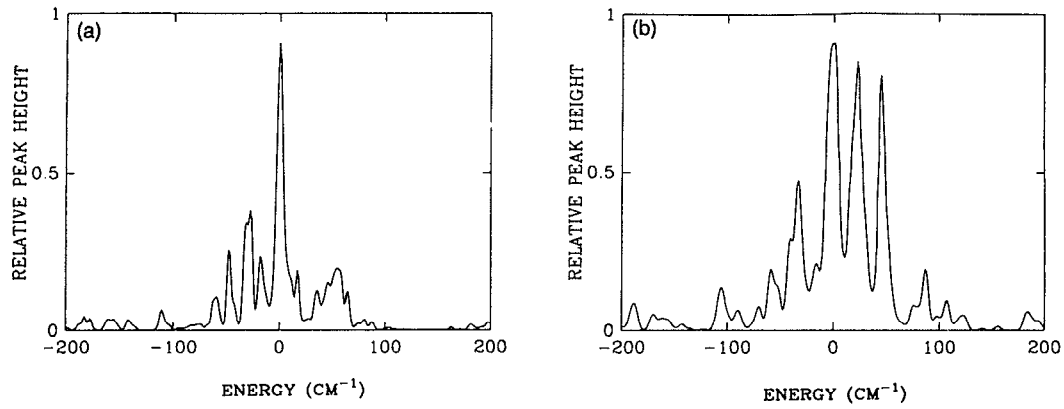

FIG. 15. Importance of quartic couplings for $v_{CH}=0$ to $v_{CH}=3$ transition of benzene: (a) with quartic couplings, (b) without quartic couplings.

spectrum is a single peak of width of 10 cm^{-1}, and other weak bands are much weaker [cf. Fig. 12(b)]. The main peak for $B=0.1$ is a superposition of three peaks (two shoulders can be observed on the red side), and the peak width is 15 cm^{-1}. The main peak for $B=0.5$ is a single peak, its width is also 10 cm^{-1}. The intensity of weak bands for $B=0.1$ is somewhat stronger than that for $B=0.5$. Results with $B=0.5$ and Eq. (6a) (solid line), compared with (6b) (dotted line), are given in Fig. 18. Results with $B=100$, i.e., $\eta\approx 1$, and Eq. (6b) are given in Fig. 19. The main spectral features are rather similar, though specific differences can be seen. The condition of $\eta\approx 1$ corresponds in Eq. (6c) to neglecting the isolated resonance weighting factor in the AI search.

A further and more detailed study of the $v_{CH}=0$ to $v_{CH}=3$ spectrum using molecular symmetry considerations more extensively is needed, and is planned. It is seen that the symmetry character of molecules plays an important role even in their overtone states, a result which, in retrospect at least, is not surprising. It can be anticipated that this combination of AI search and molecular symmetry will be very useful for study of intramolecular dynamics of other systems, and will facilitate the examination of a wider range of AI search parameters.

VI. SUMMARY

In the present study we have described what appears to be the first completely quantum mechanical calculation of vibrational transition for a real intermediate-size molecule, benzene, using the AI search. The Hamiltonian employed is based on curvilinear local-normal modes and discussed in Part I starting from Wilson's Hamiltonian. A more elaborateevaluation function for the AI search was suggested in Part II. The fundamental transition and $v_{CH}=2$ and $v_{CH}=3$ overtones were calculated. The main features of the theoretical spectra are in reasonable agreement with those of experiment.

ACKNOWLEDGMENTS

This research was supported by the Caltech Consortium in Chemistry and Chemical Engineering; Founding Members: E. I. du Pont de Neumours and Company, Inc., Eastman Kodak Company, and Minnesota Mining and Manufacturing Company. It is a pleasure to acknowledge also the support of this research by a grant from the National Science Foundation.

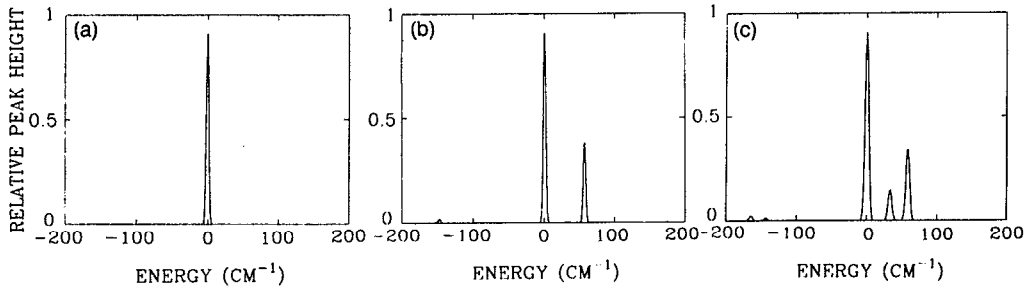

FIG. 16. Importance of kinetic couplings for $v_{CH}=0$ to $v_{CH}=1$ transition of benzene: (a) with cubic anharmonic couplings, without kinetic couplings, (b) with kinetic couplings, without cubic anharmonic couplings, and (c) with both couplings.

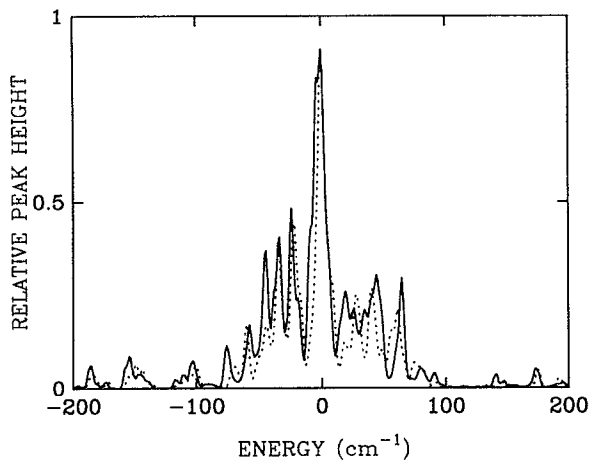

FIG. 17. A comparison for calculated spectra of $v_{CH}=0$ to $v_{CH}=3$ for benzene with $B=0.1$ (solid line) and $B=0.5$ (dotted line), using Eq. (6b) for ξ in both cases.

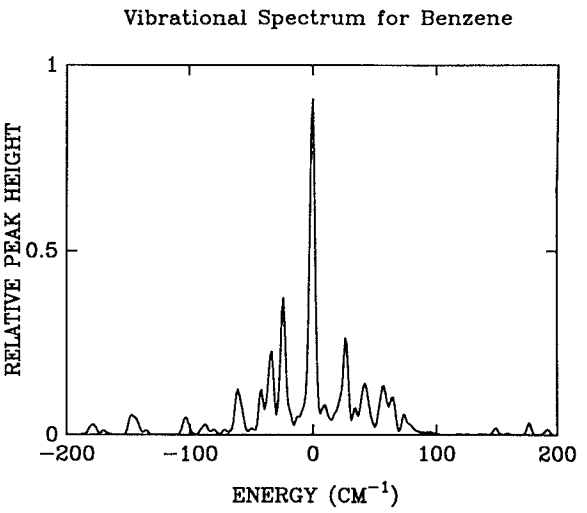

FIG. 19. The vibrational spectrum for benzene obtained with Eq. (6b) for ξ and $B=100$ i.e., $\eta\simeq 1$.

APPENDIX: BOND DIPOLE MODEL (BDM)

The spectrum of vibrational transitions may be calculated based on the bond dipole model (BDM).[28,29] The transition rate for $\psi_i \leftarrow \psi_0$ using BDM is

$$\mu_{i0}^2 \propto |\langle \psi_i|\mathbf{M}|\psi_0\rangle|^2, \tag{A1}$$

where $\mathbf{M}$ is the dipole operator in BDM,

$$\mathbf{M}=\sum_{j=1}^{l} M_j\mathbf{e}_j=\sum_{j=1}^{l} r_j \exp(-r_j/R_j^*)\mathbf{e}_j . \tag{A2}$$

Here r_j is the coordinate of the jth local mode, R_j^* is the position where the bond dipole moment of the jth local mode is a maximum, and $\mathbf{e}_j$ is a unit vector along the bond. When the vibrational motion of the bond can be described well as a Morse oscillator, with reduced mass μ and the potential function $D(1-e^{-\alpha Q})^2$, the integral in Eq. (A1) is easily calculated using the expression[28,29]

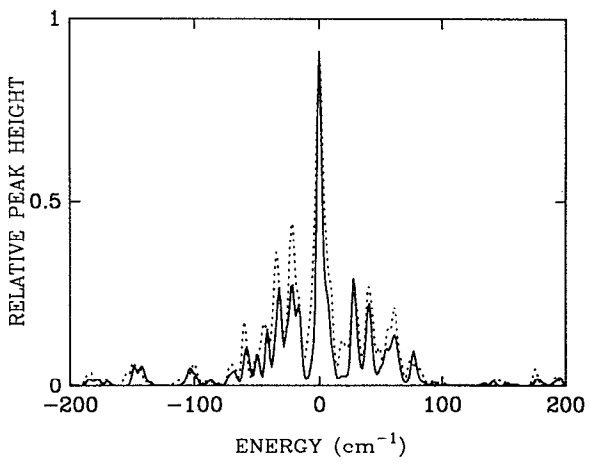

FIG. 18. The vibrational spectrum of $v_{CH}=0$ to $v_{CH}=3$ for benzene obtained with $B=0.5$ and Eq. (6a) for ξ (solid line) and (6b) for ξ (dotted line).

$$\langle v'|re^{-\alpha\lambda r}|v\rangle=\alpha^{-1}\beta^{-\lambda}e^{-\alpha\lambda R_0}[(\ln\beta+\alpha R_0)\langle v'|y^\lambda|v\rangle - d\langle v'|y^\lambda|v\rangle/d\lambda], \tag{A3}$$

where $\lambda=1/(\alpha R^*)$, R_0 is the equilibrium bond length, $y=\beta\exp(-\alpha Q)$, and $\beta=(8\mu D)^{1/2}/(\alpha\hbar)$, respectively. The analytical result for $\langle v'|y^\lambda|v\rangle$ is given by[28]

$$\langle v+j|y^\lambda|v\rangle=\tfrac{1}{\alpha}N_{v+j}N_v\sum_{l=0}^{v}\binom{l-\lambda}{l+j}\binom{l+j-\lambda}{l} \times\Gamma(\beta+\lambda-v-j-l-1)/(v-l)! \tag{A4}$$

The second term in Eq. (A3), $d\langle v'|y^\lambda|v\rangle/d\lambda$, could be calculated from Eq. (A4) by a numerical method. However, practical calculations show that the values of two terms in the right hand side of Eq. (A3) are very close to each other, so that the bracketted term in the right-hand side of Eq. (A3) is actually the difference of two large numbers and can lead to round-off problems. The analytical method seems more reliable. By combining Eq. (A4) with the following expressions:

$$\partial\binom{m}{n}/\partial m=\binom{m}{n}[\Phi(m+1)-\Phi(m-n+1)], \tag{A5}$$

$$\partial\binom{m}{n}/\partial n=\binom{m}{n}[\Phi(m-n+1)-\Phi(n+1)], \tag{A6}$$

where function Φ has its standard definition

$$\Phi(z)=d\ln\Gamma(z)/dz,$$

we have the analytical formula for $d\langle v+j|y^\lambda|v\rangle/d\lambda$ $(j\leqslant 0)$,

$$\langle v+j|y^\lambda|v\rangle =\alpha^{-1}N_{v+j}N_v\sum_{l=0}^{v}\binom{l-\lambda}{l+j}\binom{l+j-\lambda}{l}\Gamma(\beta+\lambda -v-j-l-1)/(v-l)![\Phi(1-j-\lambda)$$

$$+\Phi(1+j-\lambda)-\Phi(1+l-\lambda)$$

$$-\Phi(1+j+l-\lambda)+\Phi(\beta+\lambda-v-j-l-1)]. \quad \text{(A7)}$$

Eigenfunctions can be written as linear combinations of the zeroth-order wave functions,

$$\Psi_a=\sum_m c_{am}\Phi_m, \quad \text{(A8)}$$

where Φ_m is the product of single mode-vibrational wave functions, which are now exhibited explicitly

$$\Phi_m=\chi_1(m_1)\chi_2(m_2)\cdots\chi_s(m_s), \quad \text{(A9)}$$

where m_1, m_2,$\cdots$ are the quanta for the single mode vibrational wave functions in the mth zeroth-order wave function. Therefore, for the BDM we have

$$\langle\Psi_a|\mathbf{M}^{(k)}|\Psi_b\rangle$$

$$=\sum_{m,n,j} c_{am}c_{bn}\pi_{mn,j}\langle\chi_j(m_j)|M_j|\chi_j(n_j)\rangle e_j^{(k)}, \quad \text{(A10)}$$

where $k=x,y$ or z and

$$\pi_{mn,j}=\prod_{i\neq j}\langle\chi_i(m_i)|\chi_i(n_i)\rangle=\prod_{i\neq j}\delta_{m_in_i}. \quad \text{(A11)}$$

The R^* in Eq. (A2) appears as a parameter. In Ref. 28 a value $R^*=0.86$ Å is suggested. To simulate the fact that the ratio of intensities of vibrational spectra for v and $v+1$ varies about 1 order of magnitude, we have used $R^*=1.0$ Å.

[1] G. Herzberg, *Molecular Spectrum and Molecular Structure, Vol. II* (Van Nostrand Reinhold, New York, 1945).
[2] E. B. Wilson, Jr., J. C. Decius, and P. C. Cross, *Molecular Vibrations* (McGraw-Hill, New York, 1955).
[3] R. H. Page, Y. R. Shen, and Y. T. Lee, J. Chem. Phys. **88**, 4621, 5362 (1988); Phys. Rev. Lett. **59**, 1293 (1987).
[4] S. Brodersen and A. Langseth Mat. Fys. Skr. Dan. Vid. Selsk. **1**, 1 (1956).
[5] K. V. Reddy, D. F. Heller, and M. J. Berry, J. Chem. Phys. **76**, 2814 (1982).
[6] S. N. Thakur, L. Goodman, and A. G. Ozkabak, J. Chem. Phys. **84**, 6642 (1986).
[7] M. Scotoni, A. Boschetti, N. Oberhofer, and D. Bassi, J. Chem. Phys. **74**, 971 (1991).
[8] L. Halonen, Chem. Phys. Lett. **87**, 221 (1982).
[9] E. L. Sibert III, W. P. Reinhardt, and J. T. Hynes, J. Chem. Phys. **81**, 1115 (1984).
[10] E. L. Sibert III, J. T. Hynes, and W. P. Reinhardt, J. Chem. Phys. **81**, 1135 (1984).
[11] J. Pliva and A. S. Pine, J. Mol. Spectrosc. **126**, 82 (1987).
[12] D. H. Lu and W. L. Hase, Chem. Phys. Lett. **142**, 187 (1987).
[13] D. H. Lu and W. L. Hase, J. Phys. Chem. **92**, 3217 (1988).
[14] K. L. Bintz, D. L. Thompson, and J. W. Brady, J. Chem. Phys. **85**, 1848 (1986).
[15] D. L. Clarke and M. A. Collins, J. Chem. Phys. **86**, 6871 (1987); **87**, 5312 (1987).
[16] P. Pulay, G. Fogarasi, and J. E. Boggs, J. Chem. Phys. **74**, 3999 (1981).
[17] P. Pulay, J. Chem. Phys. **85**, 1703 (1986).
[18] A. G. Ozkabak, L. Goodman, S. N. Thakur, and K. Krogh-Jespersen, J. Chem. Phys. **83**, 6047 (1985).
[19] A. G. Ozkabak and L. Goodman, J. Chem. Phys. **87**, 2564 (1987).
[20] S. M. Lederman, S. J. Klippenstein, and R. A. Marcus, Chem. Phys. Lett. **146**, 7 (1988).
[21] S. M. Lederman and R. A. Marcus, J. Chem. Phys. **88**, 6312 (1988).
[22] Y. F. Zhang and R. M. Marcus, J. Chem. Phys. **96**, 6065 (1992). The vertical line separating the first two columns in Eqs. (A1) and (B1) was inadvertently omitted.
[23] Y. F. Zhang, S. J. Klippenstein, and R. A. Marcus, J. Chem. Phys. **94**, 7319 (1991).
[24] Y. F. Zhang and R. A. Marcus (to be submitted for publication).
[25] The currently available quadratic force constants for benzene depend upon the experimental harmonic frequencies, which in turn are obtained from fitting the experimental spectra. However, some contributions from higher power terms in the Hamiltonian (such as, the second kinetic couplings and quartic anharmonic couplings) have not been corrected in that fitting procedure. Thereby the current "harmonic frequencies" actually contain some contributions from higher power terms. For an intermediate molecule, such as benzene, with tens of vibrational modes, the accumulated error generates a shift in the zero-point energy.
[26] In Pliva and Pine's work (Ref. 11) the Herzberg's numbering system was applied and, for our purpose, the relevant terms were translated into Wilson's numbering system.
[27] Unpublished studies (to be submitted).
[28] L. Halonen, Chem. Phys. Lett. **26**, 221 (1982).
[29] I. Schek, J. Jortner, and M. L. Sage, Chem. Phys. Lett. **64**, 209 (1979).
[30] P. Pulay (private communication); N. C. Handy (private communication).